Published in final edited form as:
J Bone Miner Res. 2013 July ; 28(7): 1599–1610. doi:10.1002/jbmr.1890.

Inhibition of CaMKK2 Stimulates Osteoblast Formation and Inhibits Osteoclast Differentiation

Rachel L. Cary, BS[1], **Seid Waddell, BS**[2], **Luigi Racioppi, MD. PhD**[3,4], **Fanxin Long, PhD**[5], **Deborah V. Novack, MD. PhD**[6], **Michael J. Voor, PhD**[2], and **Uma Sankar, PhD**[1,7,#]

[1]James Graham Brown Cancer Center and Owensboro Cancer Research Program, University of Louisville, Louisville, KY 40202

[2]Department of Orthopaedic Surgery, University of Louisville, Louisville, KY 40202

[3]Department of Medicine, Duke University, Durham, NC 27705

[4]University of Naples Federico II, Naples, Italy 80131

[5]Department of Medicine, Department of Developmental Biology, Washington University School of Medicine, St. Louis, MO 63110

[6]Department of Medicine and Pathology, Washington University School of Medicine, St. Louis, MO 63110

[7]Department of Pharmacology and Toxicology, University of Louisville, Louisville, KY 40202

Abstract

Bone remodeling, a physiological process characterized by bone formation by osteoblasts (OB) and resorption of pre-existing bone matrix by osteoclasts (OC), is vital for the maintenance of healthy bone tissue in adult humans. Imbalances in this vital process result in pathological conditions including osteoporosis. Owing to its initial asymptomatic nature, osteoporosis is often detected only after the patient has sustained significant bone loss or a fracture. Hence, anabolic therapeutics that stimulates bone accrual is in high clinical demand. Here we identify Ca^{2+}/calmodulin (CaM)-dependent protein kinase kinase 2 (CaMKK2) as a potential target for such therapeutics, as its inhibition enhances OB differentiation and bone growth and suppresses OC differentiation. Mice null for CaMKK2 possess higher trabecular bone mass in their long bones, along with significantly more OBs and fewer multinuclear OCs. Whereas *Camkk2*$^{-/-}$ MSCs yield significantly higher numbers of OBs, bone marrow cells from *Camkk2*$^{-/-}$ mice produce fewer multinuclear OCs, in vitro. Acute inhibition of CaMKK2 by its selective, cell-permeable pharmacological inhibitor STO-609 also results in increased OB and diminished OC formation. Further, we find phospho-protein kinase A (PKA) and Ser^{133} phosphorylated form of cyclic adenosine monophosphate (cAMP) response element binding protein (pCREB) to be markedly elevated in OB progenitors deficient in CaMKK2. On the other hand, genetic ablation of CaMKK2 or its pharmacological inhibition in OC progenitors results in reduced pCREB as well as significantly reduced levels of its transcriptional target, nuclear factor of activated T cells c1 (NFATc1). Moreover, in vivo administration of STO-609 results in increased OBs and diminished OCs, conferring significant protection from ovariectomy (OVX)-induced osteoporosis in adult

[#]Address correspondence to Uma Sankar, Ph.D., 505 S. Hancock Street, 412 CTRB, Louisville, KY 40202, USA. Tel: 270- 691-5957, Fax: 270-685-5684, uma.sankar@louisville.edu.

Disclosures

All authors of this manuscript state that they have no conflict of interest.

The authors further state that there are no restrictions on full access for all authors to all raw data, statistical analyses and material used in the study reported in this manuscript.

mice. Overall, our findings reveal a novel function for CaMKK2 in bone remodeling and highlight the potential for its therapeutic inhibition as a valuable bone anabolic strategy that also inhibits OC differentiation in the treatment of osteoporosis.

Keywords

Ca^{2+}/calmodulin (CaM)-dependent protein kinase kinase 2; osteoblasts; osteoclasts; STO-609; protein kinase A

Introduction

The skeletal tissue stores Ca^{2+} and is responsible for maintaining the homeostatic blood levels of this vital ion. Rapid changes in extracellular levels of the Ca^{2+} ion occur in the areas of the bone juxtaposed to actively remodeling OCs and OBs and in turn, these cells are functionally modulated by these changes.[1,2] Ca^{2+} enters the cells through ligand- or voltage-gated ion channels. Alternatively, the intracellular Ca^{2+} concentration can increase through release from stores such as the endoplasmic reticulum.[3] Intracellular Ca^{2+} is a universal second messenger and its transients are immediately sensed by the ubiquitous, high-affinity, intracellular Ca^{2+} receptor, calmodulin (CaM).[4] This initiates a cascade of Ca^{2+}/CaM–mediated signaling events that culminate in changes in key cellular events such as proliferation, differentiation, survival, and metabolism.[5] In particular, Ca^{2+}/CaM complexes bind to and activate CaM kinases (CaMKs), which are a family of multifunctional Ser/Thr protein kinases that includes CaMKI, CaMKII and CaMKIV.[5] The upstream kinases, CaMKKα (I) and CaMKKβ (II) are activated through Ca^{2+}/CaM binding and in turn phosphorylate CaMKI and CaMKIV on a critical activation loop Thr resulting in their full and autonomous activation, essentially forming a CaMK cascade.[6] Of note, CaMKII, activated by Ca^{2+}/CaM binding and autophosphorylation, is not part of the CaMK signaling cascade. Further, a third substrate of CaMKK2 (not CaMKK1) was recently identified to be adenosine monophosphate activated protein kinase (AMPK), a heterotrimeric kinase that coordinates cellular energy balance.[7]

Whereas CaMKK2 is expressed abundantly in the brain, its expression in other cell types is restricted.[8] Global genetic ablation of CaMKK2 protects the mouse from diet-induced obesity, insulin resistance, glucose intolerance, and inflammatory responses.[7,9–11] These mice (*Camkk2*$^{-/-}$) possess reduced numbers of bone marrow (BM) cells without overt anomalies in hematopoiesis.[12] However, a potential role for CaMKK2 in the regulation of bone homeostasis has not yet been explored.

OBs, derived from mesenchymal stem cells (MSCs) during postnatal life, deposit the extracellular matrix or osteoid comprised primarily of type I collagen that later mineralizes to form the bone matrix.[13] Transcription factors *Runx2* and *Osterix* regulate the lineage specification and differentiation of MSCs to OBs.[13] A number of signaling pathways including those of bone morphogenetic protein (BMP), Wnt-β-catenin and parathyroid hormone (PTH)-protein kinase A (PKA) influence OB differentiation. OBs as well as osteocytes, which are mature OBs that become trapped within the bone matrix, regulate the differentiation and function of OCs by secreting macrophage colony stimulating factor (M-CSF) and receptor activator of NF-κB ligand (RANKL).[14–16]

Multinuclear OCs that resorb the bone matrix are formed by the fusion of BM cells of the monocyte/macrophage lineage through the regulation by many signaling pathways including CaMK.[17] In particular, CREB, the downstream target of CaMKIV, orchestrates the transcriptional activation of NFATc1, a master regulator of OC differentiation.[5,18] Prior to

its stimulation by RANKL, NFATc1 in BM-derived OC precursors is hyper-phosphorylated on specific Ser/Thr residues by PKA and glycogen synthase kinase and remains precluded from the cell nucleus.[19,20] RANKL initiates intracellular Ca^{2+} transients in OC precursors, resulting in the activation of the Ca^{2+}-dependent Ser/Thr phosphatase calcineurin, which dephosphorylates NFATc1and enables its nuclear translocation.[21] Furthermore, activation of the Ca^{2+}/CaM-mediated CaMKIV-CREB pathway leads to the transcriptional activation and auto-amplification of NFATc1.[18]

Whereas CaMKIV has defined roles in OC differentiation, the role of its upstream activator CaMKK2 in bone biology remains unclear.[17,19] Here we show that mice null for CaMKK2 possess enhanced trabecular bone mass in their long bones, along with significantly higher numbers of OBs and fewer multinuclear OCs. Moreover, inhibition of CaMKK2 by its selective inhibitor STO-609 results in enhanced OBs and diminished OCs in vitro and protects from OVX-induced osteoporosis in vivo.[22] Collectively, our findings uncover a novel role for CaMKK2 in bone remodeling and suggest for its inhibition to be explored as a bone accrual strategy in the treatment of osteoporosis.

Materials and methods

Mice

WT, *Camkk2*$^{-/-}$ and *Camk4*$^{-/-}$ mice (all in C57BL/6 background) were housed in the University of Louisville (UofL) Baxter II Vivarium under a 12-h light, 12-h dark cycle. Food and water were provided *ad libitum*. All care and experimental procedures were performed according to UofL Institutional Animal Care and Use Committee protocols and in compliance with NIH guidelines on the use and care of laboratory and experimental animals.

Reagents

STO-609 was purchased from TOCRIS Bioscience (Ellisville, MO) and a stock solution of 20 mM was made in 100 mM NaOH (Sigma, St. Louis, MO). MSCs were grown on MesenCult MSC Basal media along with the associated stimulatory supplements (StemCell Technologies, Vancouver, BC), supplemented with 50 U/ml penicillin/streptomycin (P/S; Invitrogen, Carlsbad, CA). OBs were differentiated in Dulbelco's Modified Eagle Media (DMEM) low glucose (Invitrogen) supplemented with P/S, 2% fetal bovine serum (FBS; Stem Cell Tech), 50 μM ascorbic acid, 10 mM β-glycerophosphate, and 10 nM dexamethasone (all from Sigma). Osteoclasts were cultured on gelatin (0.1% gelatin in water; Millipore, Billerica, MA) coated dishes in α- Minimum Essential Media (MEM) (Invitrogen) containing 10% FBS (Atlanta Biological, Lawrenceville, GA), P/S, 30 ng/ml M-CSF (R&D Systems, Minneapolis, MN), and 50 ng/ml RANKL (Peprotech, Rockhill, NJ).

Microcomputed tomography (μCT) and histomorphometric analyses

Femurs and tibias of 8-week old female WT and *Camkk2*$^{-/-}$ mice (normal and/or OVX) were excised and fixed in 4% paraformaldehyde (PFA; Polysciences, Warrington, PA) for 24 h and then transferred to 70% ethanol. μCT imaging was performed using a custom high resolution CT scanner (Actis HR225-150, BIR, Lincolnshire, IL). We collected sequential transverse μCT images of distal femurs and proximal tibiae covering a 3 mm region from the epiphysis into the metaphysis. The image-stacks were reconstructed to generate 3-dimensional images of the regions of interest at a nominal voxel resolution of 7 μm. Image analysis software (Volume Graphics, Heidelberg, Germany and ImageJ, NIH) were used to measure cancellous bone properties through total volume, bone volume fraction, trabecular separation, thickness and numbers.[23] Only the femurs were analyzed quantitatively because it was determined that the tibias of the mice contain too few trabeculae for

microarchitectural evaluation. After μCT imaging, the femurs were decalcified for 14 days in 10% EDTA in 10mM Tris-HCl (pH 7.4) at 4°C. The decalcified femurs were paraffin-embedded and sections were stained for hematoxylin and eosin (H&E) and/or tartarate-resistant acid phosphatase (TRAP) activity. Digital images at 100× or 400× magnifications were captured using the Axio Observer Z1 microscope (Carl Zeiss, Thornwood, NY). Histomorphometric quantitation was performed using AxioVision 2.0 (Carl Zeiss).[24]

Isolation, expansion and differentiation of OCs and OBs in vitro

BM was flushed from the medullary cavity of femurs and tibias from WT, *Camkk2*$^{-/-}$ and/or *Camk4*$^{-/-}$ mice using PBS containing 2% heat inactivated FBS. Typically, BM cells from n=4, age- and sex-matched mice per genotype were pooled for these in vitro experiments. To culture OBs, BM cells were plated in MesenCult media at a density of 1×10^6 cells/cm^2. After reaching confluence, cells were trypinized, re-plated at a density of 1×10^6 cells/cm^2 and OB differentiation media was added when they were 70% confluent. The presence of OBs was detected after 14 or 21 days by fixing in 4% paraformaldehyde and staining with Leukocyte Alkaline Phosphatase Kit (Sigma) or Osteogenesis Assay Kit (Millipore ECM 815). To culture OCs, BM cells were plated at a density of 3.5×10^5 cells/cm^2 on gelatin-coated dishes in αMEM supplemented with FBS, P/S, and M-CSF. On the third day, non-adherent cells were removed and osteoclastogenesis was induced by the addition of 50 ng/ml RANKL. TRAP activity was determined after 8 days using the Acid Phosphatase, Leukocyte Kit (Sigma). Where applicable, STO-609 was added at a final concentration of 2.5 μM, 24 h prior to adding OB or OC differentiation media, to WT MSCs and/or BM-derived monocytes. STO-609 was replenished every 48 h.

Quantitative real-time reverse transcription polymerase chain reaction (qRT-PCR)

Total RNA was isolated from OB and OC cultures using RNAqueous 4-PCR Kit (Ambion, Austin, TX). Following DNase treatment, cDNA was generated using High Capacity cDNA Reverse Transcription Kit (Applied Biosystems, Foster City, CA). QRT-PCR-based gene expression analysis was performed using IQ SYBR Green Supermix (BioRad Laboratories, Inc., Hercules CA) and the Bio-Rad iQ5 iCycler System. All samples were normalized to β-actin expression levels. The primers sequences used in this study are available upon request.

Immunoblot analyses

Equal amounts of protein lysates were fractionated under denaturing conditions on SDS-PAGE and transferred onto Immobilon-P membranes (Millipore, Bellerica, MA). Blocking, primary and secondary antibody incubations were performed in Tris-buffered saline (TBS) containing 5% non-fat milk. Washes were performed in TBS with 0.5% Tween-20 (Sigma). Membrane was probed with antibodies specific to CaMKK (cat. no. 610544) and CaMKIV (cat. no. 610276) (both BD Biosciences, San Jose, CA), total and phospho-CREB (Millipore; cat. no. 06-836 and 06-515), total and phospho-AMPK (Cell Signaling, Danvers, MA; cat.no. 2532s and 2535s), total and phospho-PKA (Cell Signaling; cat. no. 4782 and 5661)), OSX (Santa Cruz; cat. no. sc-22538) and β-actin (Sigma; cat. no. A5316). Horseradish peroxidase-conjugated secondary antibodies were purchased from Jackson Immunoresearch Laboratories, Inc. (West Grove, PA). Signal intensities of bands were quantified using the NIH Image J software.

Flow Cytometry

Approximately 24 hours after the addition of RANKL, OC precursors were harvested and fixed in 1% PFA. Fixed cells were resuspended in PBS containing 0.1% BSA for blocking and/or staining with 1:100 dilutions of Alexa Fluor 488 Conjugated anti-CD115 (c-fms) (eBiosciences, San Diego, CA; cat. no. 53-1152-82) and PE Conjugated anti-CD265

(RANK) (eBiosciences; cat. no. 12-6612-82). Analysis of c-fms and RANK expression was performed using BD FACSAria (BD Biosciences).

STO-609 Treatment of Ovariectomized Mice

Ten-week old female C57BL/6 WT mice were either sham operated (n=4) or ovariectomized (n=14). STO-609 stock of 20 mM was diluted 1:2000 in sterile saline solution to obtain a 10 μM working stock concentration. The OVX mice were injected with 200 μl per mouse of sterile saline (n=7) or STO-609 (n=7), through the intraperitoneal (i.p.) route, thrice a week, starting from the day after the surgery. The study was terminated at the end of 8 weeks and the long bones from these animals were harvested for μCT and histomorphometric analyses.

Statistical analysis

All data are represented as average values ± standard deviation from n≥3 experiments. For μCT measurements in the OVX study, we performed one-way ANOVA with 95% CI to determine the statistical significance of the differences in cancellous bone properties among multiple groups. For all other experiments, statistical significance from n≥3 experiments was assessed by the Student's *t*-test.

Results

Genetic ablation of CaMKK2 in mice results in higher trabecular bone mass and more OBs

We recently reported that the *Camkk2*$^{-/-}$ mice possess fewer BM cells and pale long bones when compared to normal.[12] To begin to understand the basis for the pale appearance of the long bones in mutant mice, we performed micro-computed tomography (μCT) analysis with the femurs and found a significant increase in the trabecular bone volume in the *Camkk2*$^{-/-}$ mice over WT (Fig. 1A–B, 1D). To understand whether the enhanced trabecular bone mass observed in CaMKK2 deficient mice is due to increased OB activity, we examined H&E-stained histological sections of WT and *Camkk2*$^{-/-}$ long bones (Fig. 1C). Trabecular bone surfaces in *Camkk2*$^{-/-}$ femurs were densely lined with OBs of the cuboidal morphology, whereas WT femurs possessed mostly smaller and flatter OBs (Fig. 1C, black arrows). Histomorphometric analyses indicate a 4-fold increase in the number of total OBs per bone surface in the trabecular bone of the femur in *Camkk2*$^{-/-}$ mice, compared to WT (Fig. 1D). These results indicate that CaMKK2 deficiency results in high bone mass associated with an increased number of active OBs.

Loss of CaMKK2 enhances OB differentiation from MSCs

BM-derived MSCs can be induced to differentiate into OBs when cultured in vitro in media containing ascorbic acid and dexamethasone. Consistent with our in vivo results, MSCs derived from *Camkk2*$^{-/-}$ mice yielded 3.4-fold more alkaline phosphatase positive OBs than WT (Fig. 2A). These results indicate that taken out of their BM microenvironment, *Camkk2*$^{-/-}$ MSCs still possess the ability for enhanced differentiation into OBs, suggesting a cell-intrinsic effect of CaMKK2 on this cell type.

During OB differentiation, the transcription factors Runx2 and Osterix are known to play critical roles.[13] Other molecular markers for OBs include alkaline phosphatase which is expressed throughout multiple stages of the lineage, and osteocalcin which is expressed mainly by mature OBs.[13] Consistent with our in vivo and in vitro findings, we observed a significant 5-to 7-fold increase of *Runx2* mRNA levels in *Camkk2*$^{-/-}$ OBs by days 3–14 of differentiation, over the respective levels of the transcription factor in WT OBs (Fig. 2B). Similarly, we observed a significant increase in *Osterix* mRNA of 2.5-fold on day 7 and 10-fold on day 14 of differentiation in *Camkk2*$^{-/-}$ OBs, compared to WT (Fig. 2B). Alkaline

phosphatase mRNA levels were significantly elevated by 13-fold on day 14 of differentiation in *Camkk2*$^{-/-}$ OBs (Fig. 2B). Moreover, BMP2, a known osteogenic signal, was induced by 6 fold in the mutant over control cultures at day 14 (Fig. 2B). Altogether, these data suggest that the absence of CaMKK2 triggers a "fast-track" differentiation of MSCs into OBs.

Loss of CaMKK2 increases phosphorylation of CREB and PKA in OBs

To explore the mechanism by which CaMKK2 regulates OB differentiation, we first examined its levels during normal differentiation from WT MSCs. As shown in Fig. 3, CaMKK2 is expressed in normal MSCs and becomes elevated by day 7 when cultured in OB differentiation media (Fig. 3Ai–Aii). An obvious downstream target to investigate was AMPK, as the CaMKK2-AMPK pathway plays inhibitory roles in granulopoiesis and adipogenesis.[11,12] However, levels of phospho (p) AMPK were similar between WT and *Camkk2*$^{-/-}$ MSC cultures (Fig. 3Ai–Aii), indicating that it is not impaired by CaMKK2 deletion.

Of the two other known substrates of CaMKK2, the tissue-restricted CaMKIV is a predominantly nuclear kinase that regulates gene transcription through Ser^{133} phosphorylation of CREB (pCREB), which in turn has been shown to promote OB differentiation.[5,25–27] We therefore assessed pCREB levels as an indicator of CaMKIV activity in WT and *Camkk2*$^{-/-}$ MSCs and OBs. Whereas pCREB was present in day 7 WT OBs, it was either absent or markedly down-regulated in WT MSCs or early OB progenitors (24 h in OB media) (Fig. 3A–B). In contrast, pCREB was present in *Camkk2*$^{-/-}$ MSCs and day 1 OB progenitors, and its levels were markedly elevated by day 7 in *Camkk2*$^{-/-}$ OBs (Fig. 3Ai–Aii), indicating that the loss of CaMKK2 results in enhanced pCREB in MSCs and early OBs. To understand whether CaMKIV is responsible for the increased pCREB in OBs, we assessed pCREB in *Camk4*$^{-/-}$ MSCs and OBs. Interestingly, *Camk4*$^{-/-}$ MSCs and OBs also possessed robust pCREB, indicating that CaMKIV does not directly contribute to Ser^{133} phosphorylation of CREB in OBs (Fig. 3B). These data further suggest that in OBs, phosphorylation of the Ser^{133} residue in CREB is orchestrated by another CREB kinase, and we surmised this to be PKA, a central mediator of OB differentiation.[28–30]

It is well-established that CaMKIV phosphorylates and inhibits type I adenylate cyclase, an enzyme that converts ATP into cAMP, the upstream activator of PKA.[31] Hence, we hypothesized that during normal OB differentiation, CaMKK2-CaMKIV pathway suppresses type I adenylate cyclase-cAMP mediated activation of PKA. Therefore, the PKA pathway should be de-repressed in the absence of CaMKK2-CaMKIV signaling cascade, resulting in enhanced OB differentiation. Indeed, the levels of phosphorylated form of the catalytic subunit of PKA (pPKA-C) are enhanced in *Camkk2*$^{-/-}$ MSCs and OBs (Fig. 3Ai–Aii). In further support of this idea, we do find markedly elevated pPKA-C levels in *Camk4*$^{-/-}$ OBs (Fig. 3Ci–Cii) and *Camk4*$^{-/-}$MSCs to yield 2-fold more alkaline phosphatase positive OBs than WT (Fig. 2A). Our cumulative data thus far indicate that the genetic ablation of CaMKK2 or CaMKIV triggers OB differentiation through the activation of the PKA pathway.

Pharmacological inhibition of CaMKK2 enhances OB differentiation and pPKA levels

Our data thus far indicate that MSCs derived from mice that are globally deleted for CaMKK2 undergo enhanced OB differentiation *in vitro*, suggesting a cell-intrinsic effect. Conversely, previous reports indicate a role for the hypothalamic ventromedial nuclear CaMKK2-CaMKIV-pCREB pathway in the stimulation of bone mass accrual[32]. These data beg the question of whether an acute inhibition of CaMKK2 in WT MSCs stimulates enhanced OB differentiation, as observed with *Camkk2*$^{-/-}$ MSCs.

To this end, we treated WT MSCs with STO-609, a selective and cell-permeable inhibitor of CaMKK2, at a previously demonstrated inhibitory concentration of 2.5 μM.[11] STO-609-mediated acute inhibition of CaMKK2 in WT MSCs results in a 4-fold enhancement of Alizarin Red activity and markedly elevated levels of Osterix (Fig. 4A–B). Furthermore, STO-609 treatment of WT MSCs resulted in notably enhanced pPKA-C in day 3 and 7 OB progenitors, compared to vehicle-treated cells (Fig. 4B), suggesting a positive effect of CaMKK2 inhibition on PKA activation. Altogether, our data indicate that global genetic ablation of CaMKK2 or its acute inhibition specifically in WT MSCs by STO-609 results in the activation of PKA and enhanced OB differentiation (Fig. 4C).

Loss or inhibition of CaMKK2 reduces multinuclear OCs

To understand whether the absence of CaMKK2 also affects OC differentiation, we assessed femur sections from WT and *Camkk2*$^{-/-}$ mice for TRAP activity, a histochemical marker for OCs.[15] Compared to WT, *Camkk2*$^{-/-}$ multinuclear OCs stained weakly for TRAP activity and displayed impaired attachment to the bone surface (Fig. 5A, black arrows). Histomorphometric analyses indicate that compared to WT, the long bones from *Camkk2*$^{-/-}$ mice not only possessed significantly fewer (2.4-fold) TRAP-positive OCs, but also displayed a significant reduction (8.7-fold) in the extent of trabecular bone surface contacted by the mutant OCs (Fig. 5B). To further understand the role of CaMKK2 in OC differentiation, we cultured WT and *Camkk2*$^{-/-}$ BM-derived monocytes in the presence of M-CSF and RANKL and observed a 2.2-fold reduction in the total numbers of TRAP-positive osteoclasts generated by *Camkk2*$^{-/-}$ BM cells, compared to WT (Fig. 5Ci–ii). OCs are derived from BM cells of hematopoietic origin, and *Camkk2*$^{-/-}$ mice possess decreased numbers of BM cells compared to WT.[12,14] Hence the diminished OC formation by *Camkk2*$^{-/-}$ BM cells could be due to a decrease in the numbers of c-fms/RANK expressing mutant progenitors. To understand whether this is the case, we analyzed c-FMS/RANK immunoreactivity in WT and *Camkk2*$^{-/-}$ BM-derived monocytes that were grown in the presence of M-CSF for three days and then shifted to media containing M-CSF and RANKL for 24 hours. Flow cytometric analyses reveal the presence of higher numbers of RANK-positive (3-fold) and c-fms/RANK-double positive (2-fold) population among RANKL-treated *Camkk2*$^{-/-}$ BM-derived monocytes, compared to WT (Fig. 5Ciii, lower histograms). On the other hand, we observed a moderate, but consistent decrease in c-fms-positive population in the RANKL-treated *Camkk2*$^{-/-}$ samples. Altogether these data indicate that loss of CaMKK2 does not affect the generation of c-fms/RANK-expressing OC progenitors *per se*, but may rather affect one or more subsequent steps to mediate a cell-intrinsic repression of OC differentiation.

We further analyzed the expression levels of mRNAs that are highly expressed in OCs, and observed *Acp5* (TRAP) and *CtsK* levels to be significantly down-regulated, 2-fold and 3-fold respectively in *Camkk2*$^{-/-}$ OCs, compared to WT (Fig. 5D). As mentioned earlier, *CtsK* levels in OCs are regulated by the master regulator transcription factor, NFATc1.[18] Indeed, we found the mRNA levels of *NFATc1* to be down-regulated by a significant 12.6-fold on day 3 and 3-fold on day 6 of OC differentiation respectively, compared to WT (Fig. 5D). Additionally, we observed no differences in matrix metalloproteinase 9 (*Mmp-9*) levels between WT and *Camkk2*$^{-/-}$ OCs (Fig. 5D). Altogether, these data support a model wherein the loss of CaMKK2 negatively regulates OC differentiation, perhaps through the downregulation of NFATc1.

NFATc1 is transcriptionally regulated by the CREB pathway, which in turn is a downstream target of the CaMKK2-CaMKIV pathway.[5,17] We therefore hypothesized that the levels of Ser^{133}-phosphorylated form of CREB would be down-regulated in OC progenitors lacking CaMKK2. To this end, we assessed pCREB levels in WT, *Camkk2*$^{-/-}$ *and Camk4*$^{-/-}$ OCs as well as in WT OCs treated with STO-609. Compared to RANKL-treated WT OCs,

CaMKK2 and/or CaMKIV null OCs possess markedly lower levels of pCREB (Fig. 6Ai–Aii, compare lanes 2–3, 7– 8 and 10–11 in 6Ai). Similarly, pCREB levels were reduced in STO-609-treated WT OC progenitors, indicating that the acute inhibition of CaMKK2 leads to the suppression of Ser^{133}-phosphorylation of CREB (Fig. 6Ai–Aii, compare lanes 2–3 and 4–5 in 6Ai). Next, we wanted to assess whether akin to OBs, OCs deficient in CaMKK2 or CaMKIV also express elevated pPKA-C. However, acute inhibition or genetic ablation of CaMKK2 or CaMKIV did not significantly affect pPKA levels (Fig. 6Ai–Aii, compare day 3 and day 7), indicating that the CaMKK pathway may not regulate PKA in OCs.

Our observations thus far indicate impaired OC formation by *Camkk2*$^{-/-}$ BM cells, prompting the question of whether acute inhibition of CaMKK2 in WT BM-derived monocytes will inhibit their potential for differentiation into multinucleated OCs. As indicated in Fig. 6B, pharmacological inhibition of CaMKK2 by STO-609 resulted in a significant, 4-fold reduction in the number of multinuclear TRAP-positive OCs formed by WT BM-derived monocytes. Moreover, the STO-609 treated WT OCs express significantly reduced levels of *Acp5* (3-fold) and *NFATc1* (4-fold) mRNA compared to untreated controls (Fig. 6C). Altogether, these data suggest the existence of a functional CaMKK2-CREB-NFATc1 signaling cascade in OCs, such that the genetic deletion or STO-609-mediated pharmacological inhibition of CaMKK2 results in reduced pCREB and *NFATc1* mRNA levels, leading to impaired OC differentiation (Fig. 6D).

CaMKK2 inhibition protects against ovariectomy-induced bone loss

Loss or pharmacological inhibition of CaMKK2 stimulates OBs while inhibiting OC differentiation, resulting in a net increase in bone mass. Hence, we surmised that the inhibition of CaMKK2 would protect against osteoporosis. We tested this idea in an OVX-induced model of post-menopausal osteoporosis performed in 10-week old female WT mice. Half of the ovariectomized mice were given tri-weekly intra peritoneal (i.p.) injections of STO-609 (10 μmol/kg body weight), the selective pharmacological inhibitor of CaMKK2.[7] μCT measurements indicate that after 8 weeks post-surgery, the ovariectomized WT mice suffered a 40% loss of trabecular bone volume (BV/TV) and a 35% increase in the extent of trabecular separation (Tr.Sp.), compared to sham-operated control mice (Fig. 7A–C). Treatment with STO-609 conferred significant protection from OVX-induced bone loss as the differences in BV/TV and the extent of Tr.Sp. between sham-operated control and STO-609-treated OVX mice were non-significant, whereas differences in these parameters were highly significant between STO-609 treated and untreated OVX mice (Fig. 7A–B). Further, trabecular thickness (Tr.Th), a parameter indicative of OC and OB activity, became diminished following OVX, whereas this erosion was prevented by inhibiting CaMKK2 with STO-609 (Fig. 7C).

To understand whether STO-609-mediated protection of OVX-induced bone loss resulted from enhanced OBs and reduced OCs, we performed histomorphometric analyses of femur sections from sham, OVX and STO-609-treated OVX mice. Indeed, femur sections from STO-609-treated OVX mice possessed significantly increased numbers of OBs, compared to untreated OVX (2-fold) or sham-operated control mice (Fig. 7Di) and these OBs mostly possessed a cuboidal morphology (Fig. 7Dii). These data indicate that CaMKK2 inhibition by STO-609 stimulates OBs. Further, OVX resulted in a significant increase in the number of TRAP-positive OCs as well as the extent of trabecular bone surface contacted by them (Fig. 7Di–Dii). Administration of STO-609 resulted in a significant reduction in the number of TRAP-positive OCs as well as in the extent of their contact with the bone surface (Fig. 7Di–Dii). In fact, these numbers in STO-treated OVX mice were significantly lower than those in sham-operated control mice, indicating a suppression of OC formation by STO-609. Collectively, these data indicate that STO-609, the selective inhibitor of CaMKK2, confers

protection from OVX-induced post-menopausal bone loss by stimulating OBs and bone formation as well as suppressing OCs.

Discussion

Tremendous progress in the understanding of molecular mechanisms governing bone homeostasis has led to the development of several highly efficient anti-osteoporosis drugs that mostly target OC differentiation and/or function.[33] Whereas prevention of OC-mediated bone resorption and further bone loss is critical, stimulation of OB activity and bone growth to replace the eroded bone mass is equally important in the treatment of osteoporosis. Here we report a novel role for the tissue-restricted CaMKK2 in the dual regulation of OB and OC biology. Specifically, genetic ablation of CaMKK2 in mice increases bone mass due to enhanced OB differentiation and diminished OC differentiation. Mechanistically, inhibition of CaMKK2 appears to favor osteoblastogenesis via the activation of the PKA pathway and inhibit OC differentiation through the downregulation of NFATc1. Importantly, pharmacological inhibition of CaMKK2 by STO-609 stimulates OBs and inhibits OCs and prevents bone loss in a murine OVX model. Thus, CaMKK2 inhibition may be a feasible strategy to inhibit and reverse bone loss in patients with post-menopausal osteoporosis.

Our data indicate that CaMKK2 is inhibitory to normal osteoblastogenesis. A similar phenomenon was recently reported during adipogenesis, where acute inhibition or deletion of CaMKK2 in pre-adipocytes leads to their accelerated differentiation into adipocytes.[11] Whereas the effects of CaMKK2 inhibition on adipogenesis are mediated through the AMPK-pre-adipocyte factor 1-Sox9 pathway, we find AMPK levels to be unaltered between WT and *Camkk2*$^{-/-}$ MSCs and OBs. Instead, our data indicate a potential role for CaMKK2 in OB differentiation via the suppression of the PKA pathway.

Cross-talk between the Ca^{2+} and cAMP pathways regulates several cell physiological processes.[31,34] In particular, CaMKIV and PKA antagonize each other in several cell types, including neurons, human embryonic kidney cells and OCs.[19,31,35] In neurons, CaMKIV directly phosphorylates and inhibits type I adenylate cyclase, and in OCs, it inhibits type 3 adenylyl cyclase.[19,31] PKA, on the other hand, directly phosphorylates CaMKKs on Ser^{458} in the CaM-binding domain, leading to the inhibition of the CaMKK-CaMKIV cascade.[35] Our data indicate that whereas both CaMKK2 and CaMKIV are expressed in WT MSCs and day 1 OB progenitors, phosphorylated and active forms of PKA are either absent or markedly downregulated (Fig. 3). Therefore, we propose that during normal homeostasis, CaMKK2-CaMKIV antagonizes the cAMP-PKA pathways through a “check-point” mechanism to prevent premature differentiation of MSCs into OBs (Fig. 4C). Conversely, genetic ablation or pharmacological inhibition of CaMKK2 relieves this repression, resulting in elevated levels of phosphorylated form of PKA and accelerated OB differentiation (Fig. 4C).

Our results also indicate an inhibition of OC differentiation following the inhibition or absence of CaMKK2, with concomitant down-regulation of pCREB as well as NFATc1, a Ca^{2+}/CaM-dependent transcription factor that is the master regulator of OC differentiation.[18] Based on previous studies by others, we speculate this to be a direct effect of the CaMKK2-pCREB-NFATc1 pathway (Fig. 6D). However, the exact mechanism by which CaMKK2 stimulates homeostatic osteoclastogenesis remains to be elucidated. Intriguingly, unlike in OBs, the PKA pathway is unperturbed in CaMKK2-deficient or STO-609-treated OCs. Previous studies show enhanced intracellular cAMP levels and diminished nuclear NFATc1 following the treatment of BM-derived OCs with 1μM STO-609.[19] Further, PKA inhibits OC differentiation by directly phosphorylating and

inactivating NFATc1[19,20,30] However, our data suggest a non-PKA dependent mechanism in CaMKK2 null OCs. Regardless of the mechanism, our cumulative data indicate that the absence or inhibition of CaMKK2 in BM progenitors leads to a reduction in *NFATc1, Acp5* and *CtsK* mRNA levels and inhibition of OC differentiation.

The mechanism for the significantly reduced contact of the bone surface by the mutant OCs remains to be elucidated. Although we cannot rule out a direct role for CaMKK2, it is possible that indirect mechanisms are responsible for the attachment phenotype of *Camkk2*$^{-/-}$ OCs. One possibility is that the over-crowding of the *Camkk2*$^{-/-}$ bone surface by active, cuboidal OBs precludes the OCs from gaining access to the bone surface.[36] Alternatively, akin to its role in BM macrophages, CaMKK2 may modulate OC cytoskeletal rearrangements through its regulation of the cell adhesion kinase PYK2.[9]

Loss of CaMKK2 through global genetic deletion positively influences OBs and negatively affects OCs, resulting in a net increase in bone mass. Oury et al. reported recently that brain-derived serotonin stimulates the CaMKK2-CaMKIV-pCREB pathway in the hypothalamic ventromedial nucleus which then decreases sympathetic tone and promotes bone mass accrual.[32] These data raise the possibility that the skeletal phenotype observed in *Camkk2*$^{-/-}$ mice is an indirect effect of the loss of the gene in non-skeletal tissues such as the brain. However, STO-609-mediated pharmacological inhibition of CaMKK2 in WT BM-derived MSCs accelerates OB differentiation whereas its inhibition in WT BM-derived monocytes inhibits OC differentiation (Fig. 4 and 6). Furthermore, STO-609 treatment protects mice from OVX-induced bone loss by stimulating OBs and inhibiting OCs (Fig. 7). Altogether, these data support a cell-intrinsic role for CaMKK2 in OB and OC differentiation and bone remodeling.

CaMKK2 is tissue-restricted and its loss protects mice from diet-induced obesity, insulin resistance, glucose intolerance, and inflammatory responses.[7–11] As therapies that stimulate OB differentiation and activity while suppressing OCs are in high clinical demand, CaMKK2 inhibition could be explored as a safe and effective dual-action therapeutic strategy against osteoporosis that promotes robust bone growth while inhibiting resorption.

Acknowledgments

The authors thank Dr. Anthony R. Means for his kind gift of *Camkk2*$^{-/-}$ and *Camk4*$^{-/-}$ mice; and advice. We thank Janice Ditslear for help with animal surgeries and i.p. injections. This study was supported by a Department of Defense USAMRMC research grant (W81XWH-10-2-0082-CLIN 1) and JGBCC and OCRP funds to US. DVN is supported by AR052705 (NIAMS). MJV is supported by a grant from the Kentucky Science and Engineering Foundation. Histological analysis was supported in part by The Center for Musculoskeletal Biology and Medicine at Washington University, P30AR057235 (NIAMS).

References

1. Harada S, Rodan GA. Control of osteoblast function and regulation of bone mass. Nature. 2003; 423(6937):349–355. [PubMed: 12748654]
2. Xia S-L, Ferrier J. Localized calcium signaling in multinucleated osteoclasts. Journal of cellular physiology. 1996; 167(1):148–155. [PubMed: 8698832]
3. Ghosh A, Greenberg ME. Calcium signaling in neurons: molecular mechanisms and cellular consequences. Science. 1995; 268(5208):239–247. [PubMed: 7716515]
4. Lu KP, Means AR. Regulation of the cell cycle by calcium and calmodulin. Endocr Rev. 1993; 14(1):40–58. [PubMed: 8491154]
5. Colomer J, Means AR. Physiological roles of the Ca2+/CaM-dependent protein kinase cascade in health and disease. Subcell Biochem. 2007; 45:169–214. [PubMed: 18193638]
6. Means AR. The Year in Basic Science: calmodulin kinase cascades. Molecular endocrinology. 2008; 22(12):2759–2765. [PubMed: 18845671]

7. Anderson KA, Ribar TJ, Lin F, Noeldner PK, Green MF, Muehlbauer MJ, Witters LA, Kemp BE, Means AR. Hypothalamic CaMKK2 Contributes to the Regulation of Energy Balance. Cell Metabolism. 2008; 7(5):377–388. [PubMed: 18460329]
8. Racioppi L, Means AR. Calcium/Calmodulin-Dependent Protein Kinase Kinase 2: Roles in Signaling and Pathophysiology. J Biol Chem. 2012
9. Racioppi L, Noeldner PK, Lin F, Arvai S, Means AR. Calcium/Calmodulin-dependent Protein Kinase Kinase 2 Regulates Macrophage-mediated Inflammatory Responses. J Biol Chem. 2012; 287(14):11579–11591. [PubMed: 22334678]
10. Anderson KA, Lin F, Ribar TJ, Stevens RD, Muehlbauer MJ, Newgard CB, Means AR. Deletion of CaMKK2 from the liver lowers blood glucose and improves whole-body glucose tolerance in the mouse. Mol Endocrinol. 2012; 26(2):281–291. [PubMed: 22240810]
11. Lin F, Ribar TJ, Means AR. The Ca2+/Calmodulin-Dependent Protein Kinase Kinase, CaMKK2, Inhibits Preadipocyte Differentiation. Endocrinology. 2011
12. Teng EC, Racioppi L, Means AR. A cell-intrinsic role for CaMKK2 in granulocyte lineage commitment and differentiation. Journal of leukocyte biology. 2011
13. Long F. Building strong bones: molecular regulation of the osteoblast lineage. Nat Rev Mol Cell Biol. 2011; 13(1):27–38. [PubMed: 22189423]
14. Novack DV, Teitelbaum SL. The Osteoclast: Friend or Foe? Annual Review of Pathology: Mechanisms of Disease. 2008; 3(1):457–484.
15. Sankar U, Patel K, Rosol TJ, Ostrowski MC. RANKL coordinates cell cycle withdrawal and differentiation in osteoclasts through the cyclin-dependent kinase inhibitors p27KIP1 and p21CIP1. J Bone Miner Res. 2004; 19(8):1339–1348. [PubMed: 15231022]
16. Nakashima T, Hayashi M, Fukunaga T, Kurata K, Oh-Hora M, Feng JQ, Bonewald LF, Kodama T, Wutz A, Wagner EF, Penninger JM, Takayanagi H. Evidence for osteocyte regulation of bone homeostasis through RANKL expression. Nat Med. 2011; 17(10):1231–1234. [PubMed: 21909105]
17. Sato K, Suematsu A, Nakashima T, Takemoto-Kimura S, Aoki K, Morishita Y, Asahara H, Ohya K, Yamaguchi A, Takai T, Kodama T, Chatila TA, Bito H, Takayanagi H. Regulation of osteoclast differentiation and function by the CaMK-CREB pathway. Nat Med. 2006; 12(12):1410–1416. [PubMed: 17128269]
18. Negishi-Koga T, Takayanagi H. Ca2+-NFATc1 signaling is an essential axis of osteoclast differentiation. Immunological reviews. 2009; 231(1):241–256. [PubMed: 19754901]
19. Yoon S-H, Ryu Jy, Lee Y, Lee ZH, Kim H-H. Adenylate cyclase and calmodulin-dependent kinase have opposite effects on osteoclastogenesis by regulating the PKA-NFATc1 pathway. Journal of Bone and Mineral Research. 2011; 26(6):1217–1229. [PubMed: 21611964]
20. Sheridan CM, Heist EK, Beals CR, Crabtree GR, Gardner P. Protein kinase A negatively modulates the nuclear accumulation of NF-ATc1 by priming for subsequent phosphorylation by glycogen synthase kinase-3. J Biol Chem. 2002; 277(50):48664–48676. [PubMed: 12351631]
21. Takayanagi H, Kim S, Koga T, Nishina H, Isshiki M, Yoshida H, Saiura A, Isobe M, Yokochi T, Inoue J, Wagner EF, Mak TW, Kodama T, Taniguchi T. Induction and activation of the transcription factor NFATc1 (NFAT2) integrate RANKL signaling in terminal differentiation of osteoclasts. Dev Cell. 2002; 3(6):889–901. [PubMed: 12479813]
22. Tokumitsu H, Inuzuka H, Ishikawa Y, Ikeda M, Saji I, Kobayashi R. STO-609, a specific inhibitor of the Ca(2+)/calmodulin-dependent protein kinase kinase. J Biol Chem. 2002; 277(18):15813–15818. [PubMed: 11867640]
23. Bouxsein ML, Boyd SK, Christiansen BA, Guldberg RE, Jepsen KJ, Müller R. Guidelines for assessment of bone microstructure in rodents using micro–computed tomography. Journal of Bone and Mineral Research. 2010; 25(7):1468–1486. [PubMed: 20533309]
24. Parfitt AM, Drezner MK, Glorieux FH, Kanis JA, Malluche H, Meunier PJ, Ott SM, Recker RR. Bone histomorphometry: Standardization of nomenclature, symbols, and units: Report of the asbmr histomorphometry nomenclature committee. Journal of Bone and Mineral Research. 1987; 2(6):595–610. [PubMed: 3455637]

25. Wang SL, Ribar TJ, Means AR. Expression of Ca(2+)/calmodulin-dependent protein kinase IV (caMKIV) messenger RNA during murine embryogenesis. Cell Growth Differ. 2001; 12(7):351–361. [PubMed: 11457732]
26. Swarthout JT, D'Alonzo RC, Selvamurugan N, Partridge NC. Parathyroid hormone-dependent signaling pathways regulating genes in bone cells. Gene. 2002; 282(1–2):1–17. [PubMed: 11814673]
27. Swarthout JT, Tyson DR, Jefcoat SC Jr, Partridge NC. Induction of transcriptional activity of the cyclic adenosine monophosphate response element binding protein by parathyroid hormone and epidermal growth factor in osteoblastic cells. J Bone Miner Res. 2002; 17(8):1401–1407. [PubMed: 12162494]
28. Shaywitz AJ, Greenberg ME. CREB: a stimulus-induced transcription factor activated by a diverse array of extracellular signals. Annu Rev Biochem. 1999; 68:821–861. [PubMed: 10872467]
29. Tyson DR, Swarthout JT, Partridge NC. Increased osteoblastic c-fos expression by parathyroid hormone requires protein kinase A phosphorylation of the cyclic adenosine 3',5'-monophosphate response element-binding protein at serine 133. Endocrinology. 1999; 140(3):1255–1261. [PubMed: 10067851]
30. Zhang R, Edwards JR, Ko SY, Dong S, Liu H, Oyajobi BO, Papasian C, Deng HW, Zhao M. Transcriptional regulation of BMP2 expression by the PTH-CREB signaling pathway in osteoblasts. PLoS ONE. 2011; 6(6):e20780. [PubMed: 21695256]
31. Wayman GA, Wei J, Wong S, Storm DR. Regulation of type I adenylyl cyclase by calmodulin kinase IV in vivo. Mol Cell Biol. 1996; 16(11):6075–6082. [PubMed: 8887637]
32. Oury F, Yadav VK, Wang Y, Zhou B, Liu XS, Guo XE, Tecott LH, Schutz G, Means AR, Karsenty G. CREB mediates brain serotonin regulation of bone mass through its expression in ventromedial hypothalamic neurons. Genes & Development. 2010; 24(20):2330–2342. [PubMed: 20952540]
33. Rachner TD, Khosla S, Hofbauer LC. Osteoporosis: now and the future. Lancet. 2011; 377(9773): 1276–1287. [PubMed: 21450337]
34. Cao W, Sohail M, Liu G, Koumbadinga GA, Lobo VG, Xie J. Differential effects of PKA-controlled CaMKK2 variants on neuronal differentiation. RNA Biol. 2011; 8(6):1061–1072. [PubMed: 21957496]
35. Wayman GA, Tokumitsu H, Soderling TR. Inhibitory cross-talk by cAMP kinase on the calmodulin-dependent protein kinase cascade. J Biol Chem. 1997; 272(26):16073–16076. [PubMed: 9195898]
36. Karsdal MA, Fjording MS, Foged NT, Delaisse JM, Lochter A. Transforming growth factor-beta-induced osteoblast elongation regulates osteoclastic bone resorption through a p38 mitogen-activated protein kinase- and matrix metalloproteinase-dependent pathway. J Biol Chem. 2001; 276(42):39350–39358. [PubMed: 11477097]

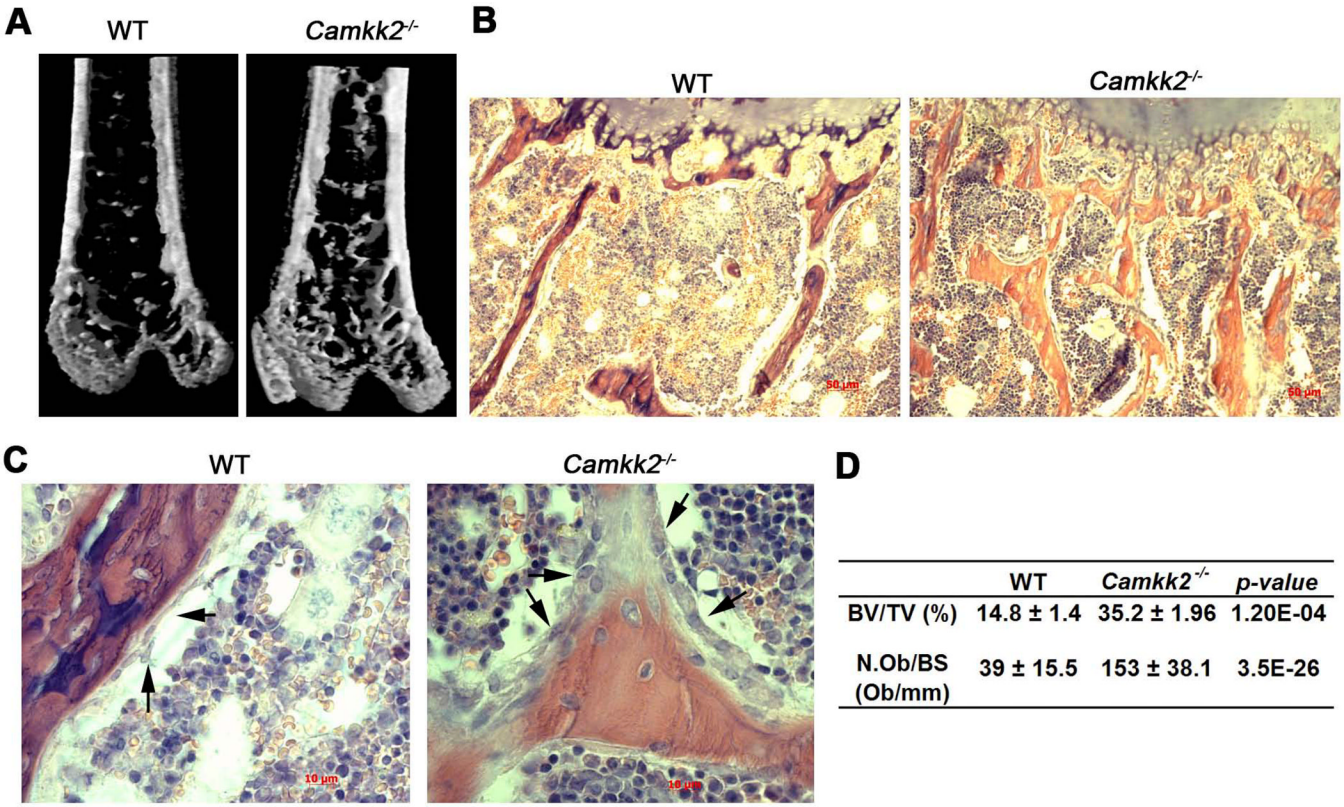

	WT	*Camkk2*$^{-/-}$	*p-value*
BV/TV (%)	14.8 ± 1.4	35.2 ± 1.96	1.20E-04
N.Ob/BS (Ob/mm)	39 ± 15.5	153 ± 38.1	3.5E-26

Figure 1. *Camkk2*$^{-/-}$ mice possess elevated bone mass and significantly more OBs in their long bones

(A) Digital μCT images of distal femurs showing enhanced trabecular bone in *Camkk2*$^{-/-}$ mice. (B) H&E stained 5μm longitudinal sections of WT and *Camkk2*$^{-/-}$ femurs at 10× magnification showing increased trabecular bone in *Camkk2*$^{-/-}$ mice. (C) Digital images (20× magnification) from H&E stained WT and *Camkk2*$^{-/-}$ femur sections depicting OBs (Black arrows). *Camkk2*$^{-/-}$ mice possess numerous cuboidal OBs bordering the trabecular bone, whereas the WT OBs possess a flatter morphology and appear to be fewer in number. (D) Table depicting bone volume per total volume (BV/TV; %) and number of OBs per bone surface (N.Ob/BS; Ob/mm) in WT and *Camkk2*$^{-/-}$ femurs measured by μCT and histomorphometric analyses respectively, from n≥8 female mice per genotype.

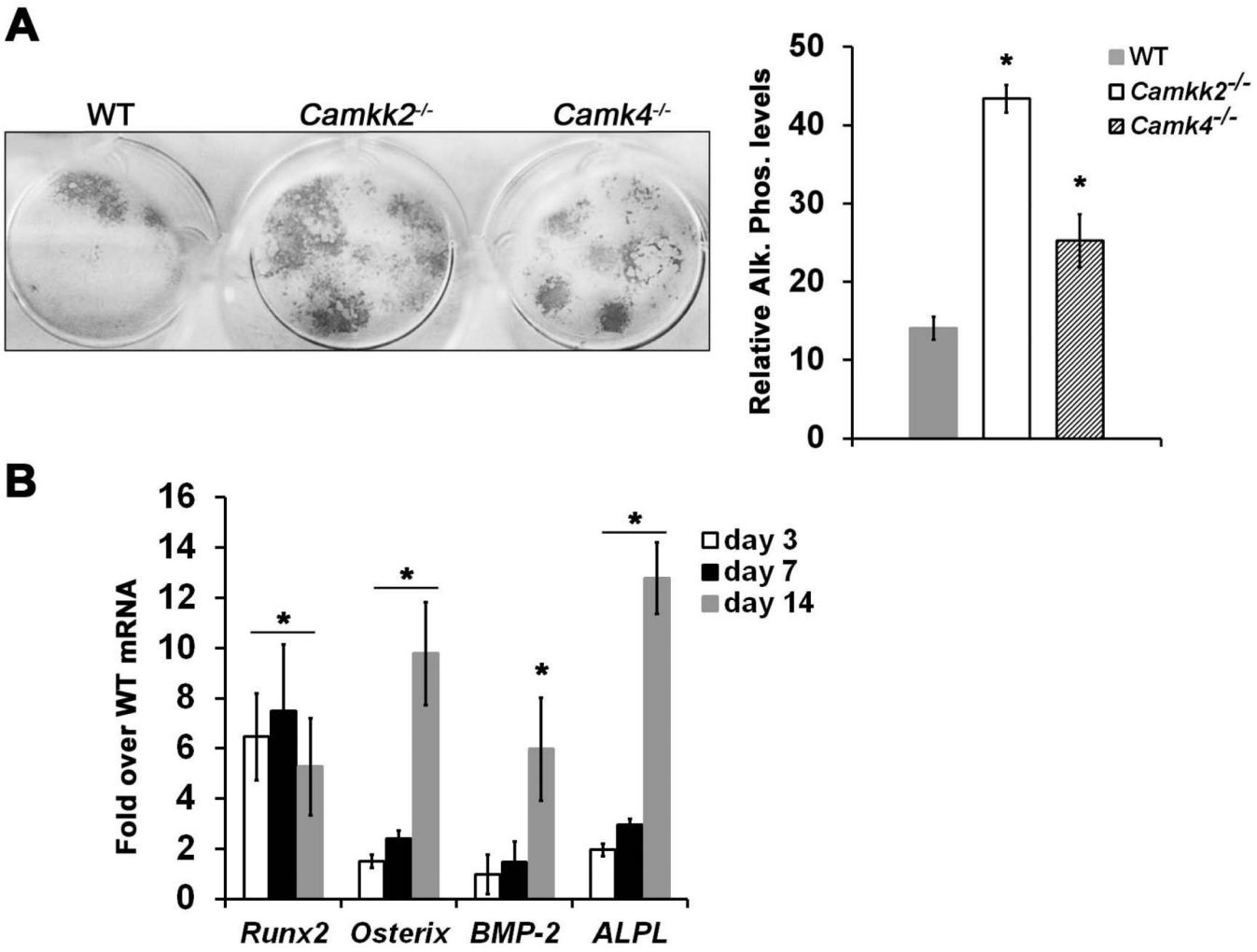

Figure 2. Genetic ablation of CaMKK2 triggers accelerated differentiation of progenitors into OBs

(A) Left: Digital images of alkaline phosphatase positivity in cultures of WT, *Camkk2*$^{-/-}$ and *Camk4*$^{-/-}$ BM-derived MSCs grown for 14 days in OB differentiation media. Right: Quantification of the relative alkaline phosphatase positivity calculated from n=3 experiments. (B) *Runx2, osterix, BMP2* and Alkaline phosphatase (*ALPL*) mRNA levels were determined from total RNA extracts prepared on indicated time points from WT and *Camkk2*$^{-/-}$ BM-derived MSCs grown for 14 days in OB media. The mRNA levels of individual genes were normalized to β-actin. Data are represented as fold induction of individual mRNA in *Camkk2*$^{-/-}$ OBS over the corresponding levels in WT OBs, at the indicated time points. Average from n=3 experiments shown; * p-value < 0.05, compared to WT.

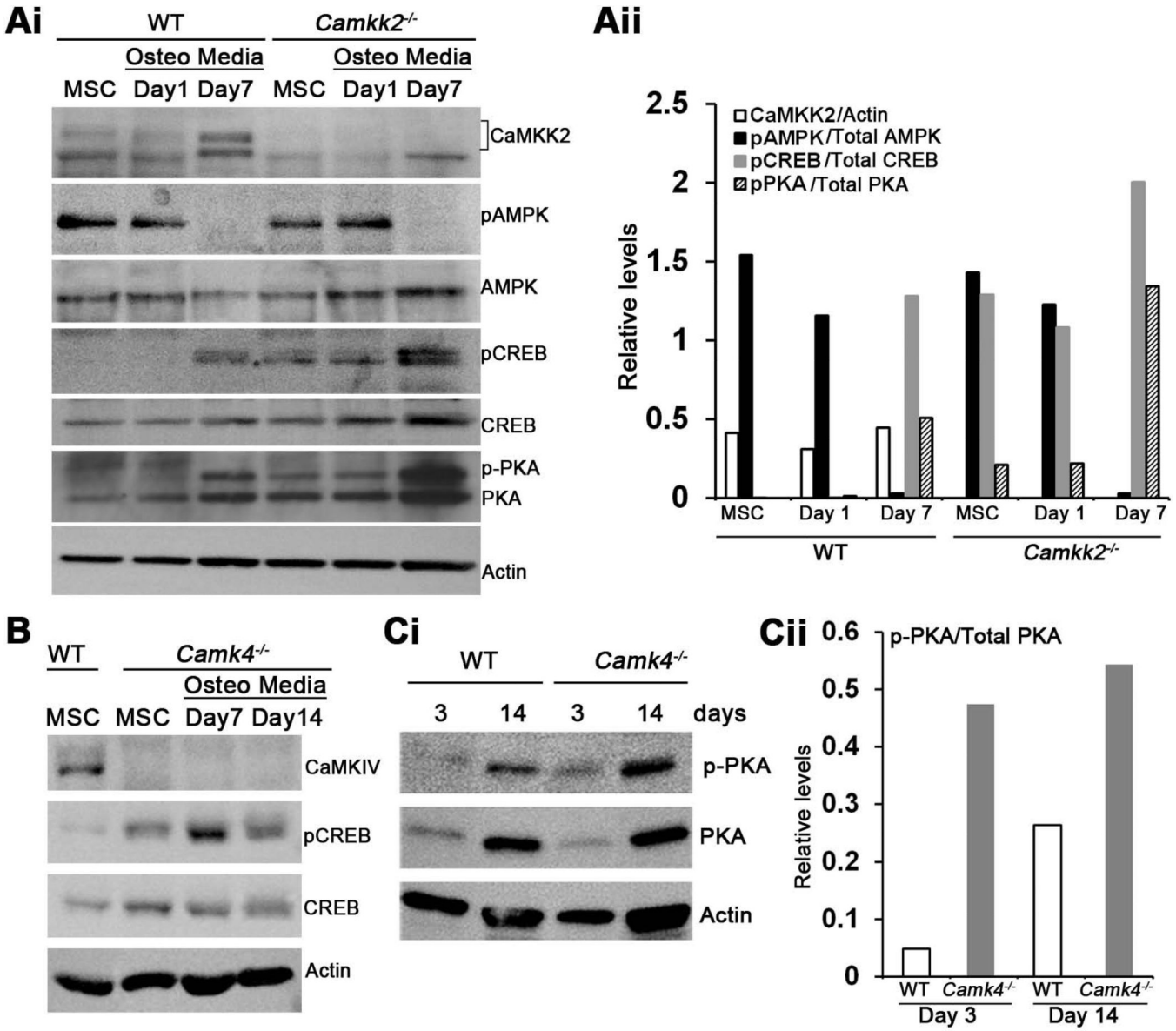

Figure 3. Absence of CaMKK2 or CaMKIV results in elevated levels of phosphorylated PKA-C and CREB

(Ai) Immunoblots were prepared of cell extracts from WT and *Camkk2*$^{-/-}$ BM-derived MSCs grown in MesenCult media or in OB media for 1 or 7 days, and probed for CaMKK2, phospho- and total AMPK, phospho- and total CREB, phospho- and total PKA (catalytic subunit) as well as actin. One representative blot from n>3 independent experiments is shown. (Aii) Relative signal intensities, calculated using the Image J software (NIH), are represented as a ratio of individual bands over the respective actin levels (CaMKK2) or those of the levels of the un-phosphorylated form of the respective proteins (AMPK, CREB and PKA-C). Signal levels from a representative immunoblot are shown. Similar results were observed in n=4 independent experiments. (B) Immunoblots depicting levels of CaMKIV, actin, phospho- and total CREB in extracts from WT and *Camk4*$^{-/-}$ MSCs or OB progenitors. Representative blot from n=3 experiments is shown. (C) Cell extracts from WT and *Camk4*$^{-/-}$ OB progenitors grown for 3 or 14 days in OB media were immunoblotted and probed for actin, phospho-and total PKA (catalytic subunit). (Cii) Relative signal intensities

of phospho/total PKA-C levels from the representative immunoblot. Similar results were observed in three independent experiments.

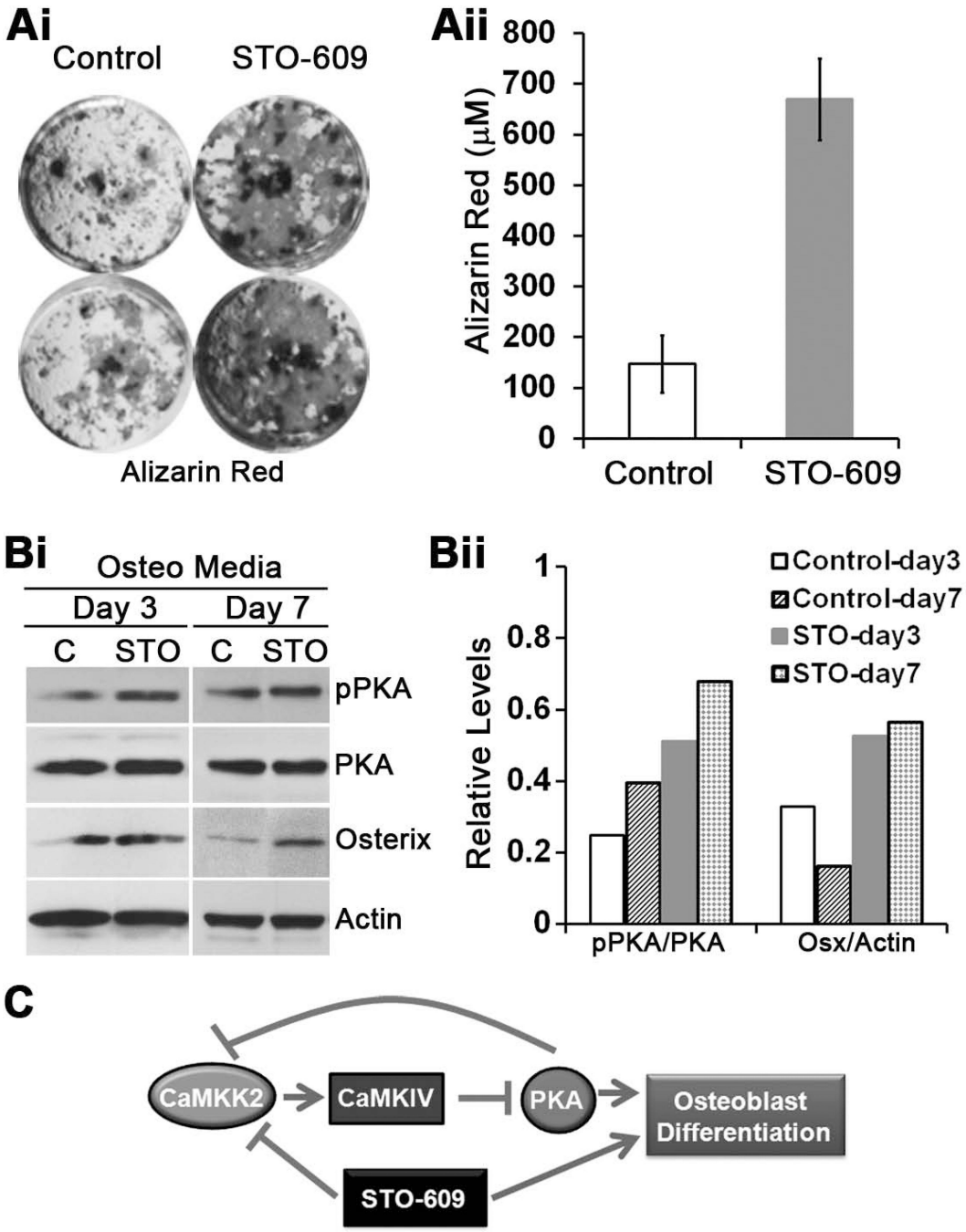

Figure 4. Pharmacological inhibition of CaMKK2 by STO-609 elevates pPKA and stimulates OB formation

(Ai) Representative digital images of alizarin red staining in cultures of WT BM-derived MSCs grown for 21 days in OB differentiation media in the absence (Control) or presence of 2.5 μM STO-609. (Aii): Quantification of the alizarin red staining calculated from n=3 experiments. (Bi) Protein extracts from WT OB progenitors grown for 3 or 7 days in OB media in the absence (Control) or presence of 2.5 μM STO-609 were immunoblotted and probed for actin, phospho-and total PKA (catalytic subunit) and Osterix. (Bii) Relative signal intensities of phospho/total PKA-C and Osterix/Actin levels from the representative immunoblots are shown. Similar results were observed in three independent experiments.

(C) During normal homeostasis, CaMKK2-CaMKIV antagonizes the cAMP-PKA pathway as a “check-point” mechanism to prevent premature differentiation of MSCs into OBs. Pharmacological inhibition of CaMKK2 by STO-609 relieves this repression, resulting in accelerated OB differentiation

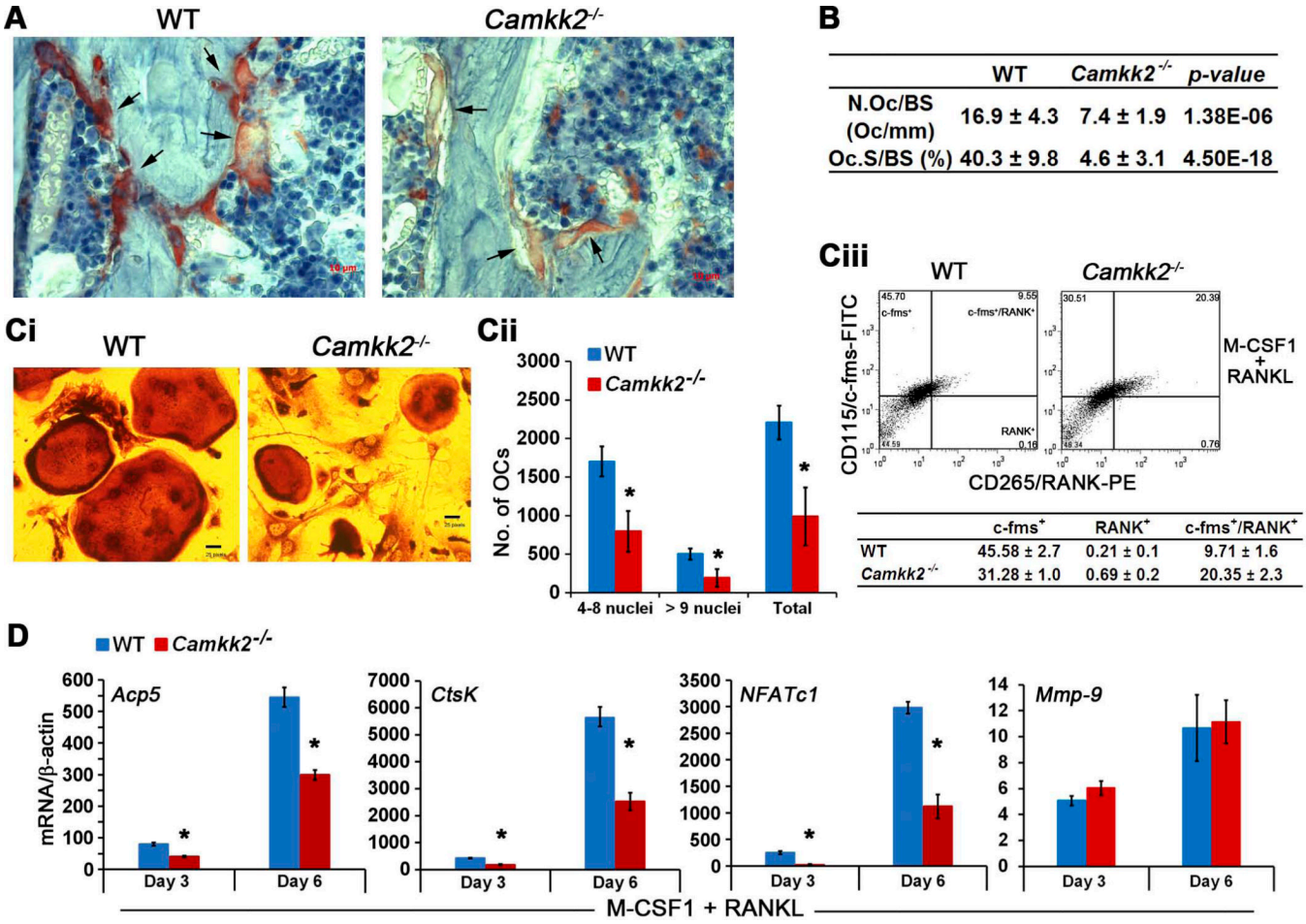

Figure 5. Loss of CaMKK2 results in a significant downregulation of OC differentiation

(A) Digital images (200× magnification) from TRAP and hematoxylin-stained 5 μm longitudinal femur sections from WT and *Camkk2*$^{-/-}$ mice depicting OCs (black arrows). Note that the *Camkk2*$^{-/-}$ OCs stain weakly for TRAP activity and appear impaired in their attachment to the bone surface. (B) Table depicting histomorphometric measurements assessing OC numbers (N.OC/BS; number of OCs per mm) and attachment to the bone surface (Oc.S/BS; %). (Ci) TRAP^{+} day 8 OCs from WT and *Camkk2*$^{-/-}$BM precursors cultured in the presence of M-CSF1 and RANKL. (Cii) Enumeration of TRAP^{+} OCs from indicated genotypes and classified per number of nuclei based on hematoxylin staining; n=3. * *p*-value < 0.0002, compared to WT. (Ciii) Representative flow cytometry histograms (n=3) depicting CD115/c-fms-FITC and CD265/RANK-PE positive populations in WT and *Camkk2*$^{-/-}$ BM-derived monocytes that were cultured for 24 h in the presence of M-CSF1 and RANKL. The cells were first live-gated on forward and side scatter plots. Table below the histograms shows average of c-fms+, RANK+ and c-fms/RANK-double positive populations (%) ± standard deviation from 3 independent experiments. (D) Normalized (to β-actin) levels of *Acp5, Ctsk, NFATc1* and *Mmp-9* mRNA in WT and *Camkk2*$^{-/-}$ OCs from days 3, and 6 of differentiation in the presence of M-CSF and RANKL; n=3. Data are presented as fold over M-CSF-only controls and show markedly lower levels of *Acp5, Ctsk, NFATc1* and normal levels of *Mmp-9* in *Camkk2*$^{-/-}$ OCs, compared to WT. * *p*-value < 0.005, compared to WT.

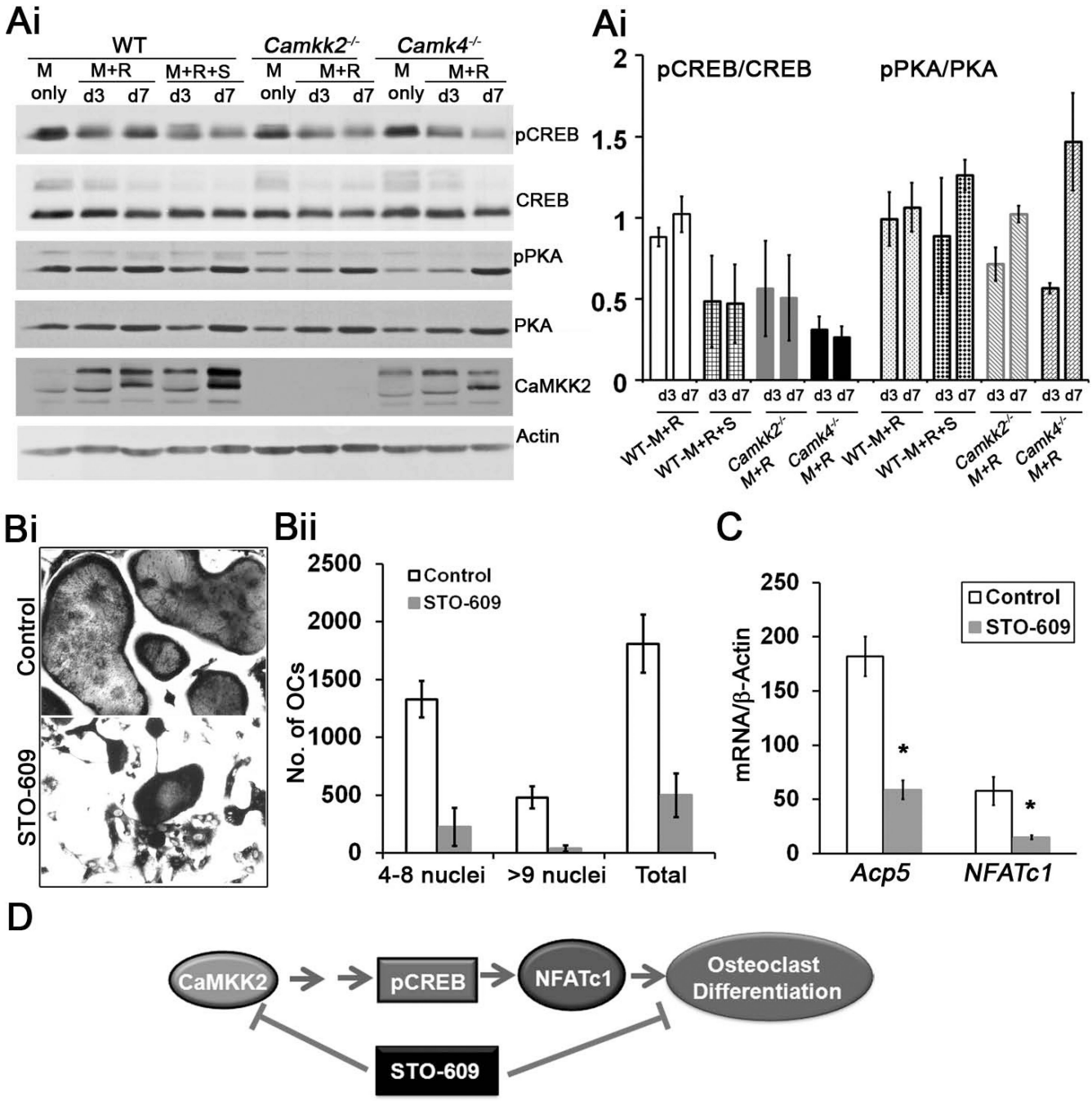

Figure 6. Acute inhibition of CaMKK2 by STO-609 results in diminished OC formation accompanied by lower levels of pCREB and NFATc1 mRNA

(Ai) Immunoblots were prepared of cell extracts from WT, *Camkk2*$^{-/-}$ and *Camk4*$^{-/-}$ BM-derived monocytes grown in BM-derived monocytes that were cultured in M-CSF1 alone (M) or in the presence of M-CSF1 and RANKL (M+R) for 3 (d3) or 7 (d7) days. For acute inhibition of CaMKK2, STO-609 was added to a final concentration of 2.5 μM, 24 h prior to the addition of differentiation media and replenished every 48 h. Immunoreactivity against CaMKK2, phospho- and total CREB, phospho- and total PKA (catalytic subunit) as well as actin are indicated from one representative blot from n=3 independent experiments. (Ai) Average signal intensities of phospho/total CREB and phospho/total PKA-C levels 3

immunoblots are shown. (Bi) $TRAP^+$ day 8 OCs from WT BM progenitors differentiated in the presence of M-CSF1 and RANKL, +/− treatment with 2.5 μM STO-609. (Bii) Enumeration of $TRAP^+$ OCs from control or STO-609-treated samples and classified per number of nuclei based on hematoxylin staining; n=3. (C) Normalized (to β-actin) levels of *Acp5* and *NFATc1* mRNA in control and STO-609-treated OCs from days 3 of differentiation in the presence of M-CSF and RANKL; n=3. * *p*-value < 0.05. (D) We hypothesize that during normal homeostasis, the CaMKK2-pCREB-NFATc1 pathway positively influences OC differentiation. Genetic ablation of pharmacological inhibition of CaMKK2 through STO-609 results in the inhibition of this pathway and OC formation.

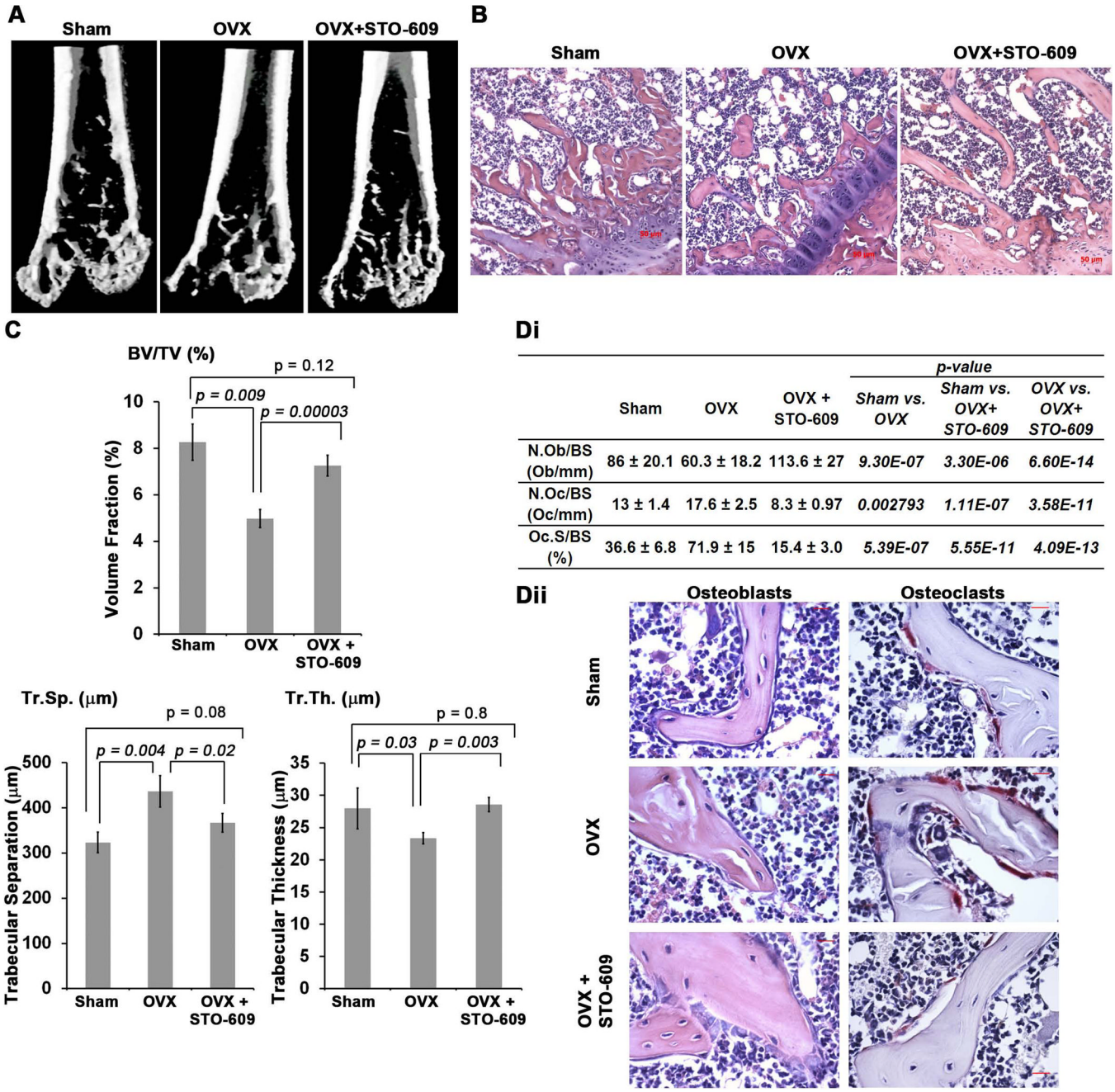

	Sham	OVX	OVX + STO-609	p-value: Sham vs. OVX	p-value: Sham vs. OVX+ STO-609	p-value: OVX vs. OVX+ STO-609
N.Ob/BS (Ob/mm)	86 ± 20.1	60.3 ± 18.2	113.6 ± 27	*9.30E-07*	*3.30E-06*	*6.60E-14*
N.Oc/BS (Oc/mm)	13 ± 1.4	17.6 ± 2.5	8.3 ± 0.97	*0.002793*	*1.11E-07*	*3.58E-11*
Oc.S/BS (%)	36.6 ± 6.8	71.9 ± 15	15.4 ± 3.0	*5.39E-07*	*5.55E-11*	*4.09E-13*

Figure 7. CaMKK2 inhibition with STO-609 protects against OVX-induced osteoporosis

(A) Representative three-dimensional digital μCT images of distal femurs from sham-operated, untreated WT-OVX and STO-609-treated WT-OVX mice at 8 weeks post-surgery. Whereas femurs from untreated OVX mice show diminished cancellous bone, those from sham control and STO-609-treated OVX mice show similar amount of cancellous bone. (B) H&E stained sections of femurs from representative sham, OVX and STO-609-treated OVX mice at 100× magnification. (C) μCT analysis of BV/TV (%), Tr. Sp. (m) and Tr. Th. (m) parameters from sham control, untreated and STO-609-treated OVX WT femurs. Average of measurements from n=4 mice per group is shown. (Di) Table depicting histomorphometric measurements assessing N.Ob/BS (Ob/mm), N.OC/BS (OC/mm) and Oc.S/BS (%) from

H&E or TRAP-stained femurs of sham control (n=4), untreated OVX (n=7) and STO-609-treated OVX (n=7) mice. (Dii) Representative H&E and TRAP stained femurs sections from representative sham, OVX and STO-609-treated OVX mice at 400× magnification showing OBs and OCs, respectively.